Science Advances
AAAS

advances.sciencemag.org/cgi/content/full/7/18/eabe5112/DC1

Supplementary Materials for

Metaform optics: Bridging nanophotonics and freeform optics

Daniel K. Nikolov, Aaron Bauer, Fei Cheng, Hitoshi Kato, A. Nick Vamivakas*, Jannick P. Rolland*

*Corresponding author. Email: nick.vamivakas@rochester.edu (A.N.V.); rolland@optics.rochester.edu (J.P.R.)

Published 30 April 2021, *Sci. Adv.* **7**, eabe5112 (2021)
DOI: 10.1126/sciadv.abe5112

This PDF file includes:

Supplementary Text

The biggest challenge in the metaform fabrication was the electron-beam lithography (EBL) writing on a curved substrate due to the demanding system specifications that were pushing the limits of the available equipment. The fabrication steps listed in the Materials and Methods section were a result of a trial and error assessment process aiming to achieve the desired local and global position of the nano-tokens with respect to the freeform substrate. Figure 3B in the main text shows one of those trial runs (referred to below as Gen 1) in which the metasurface was not properly clocked to the toroid X and Y axes of the freeform substrate (global position error), and there were stitching errors and missing tokens (local position error). To better understand the source of these errors and how they affect the imaging performance, we analyzed and compared three different metaform samples – two unsuccessful ones (Gen 1 and Gen 2) and a successful one (Gen 3). Figure S3 shows the images from the miniature imager when using each of these metaforms.

The images collected using the Gen 1 sample show performance degradation from two main fabrication errors – a rotational misalignment between the substrate and the metasurface and stitching errors between the different writing fields. If the toroid substrate and the conforming metasurface are not correctly written, additional astigmatism and other higher-order aberrations are introduced to the system. This finding explains the double-imaging and why the images are narrower in the X direction versus the Y direction. The writing field used in this example is 62.5 μm by 62.5 μm. However, due to improper calibration of the focusing parameters of the electrically actuated focusing lens, each writing zone was smaller than 62.5 μm, resulting in stitching/focusing errors with a width of ~1.5 μm. These stitching errors explain the grid-like artifacts in the final images. Additional errors in the focusing height for each writing zone were caused by the hysteresis effect (the focal length response of the lens lags behind the provided voltage input for each height setting) in the focusing lens (*52*) due to the large required refocusing range. The accumulated focusing errors also resulted in some of the smaller tokens (with dimensions < 60 nm) not being resolved, additionally decreasing the optical performance.

For the Gen 2 metaform, there was a minimal rotational misalignment between the metasurface and the substrate (±1º). An objective lens with a higher maximum FOV was used, resulting in writing areas of 1 mm by 1 mm. For a metasurface of 2 mm by 1.5 mm, four writing zones were required (2 by 2). Similar stitching/focusing errors were observed as in Gen 1, but in this case, they were thicker (~30 μm), and there were only one horizontal and one vertical line. As seen in Fig. S3, those two stitching errors propagated to the final image in the form of a cross-like artifact. Due to the larger focusing errors, most tokens did not have sharp edges (oval instead of rectangular shape), and some of the smaller tokens were not resolved at all. These defects additionally decreased the optical performance of the final image.

As can be seen from the two examples, the focusing errors caused by improper calibration and the hysteresis of the objective lens drastically decreased the optical performance of the system. Stitching errors and missing or badly resolved nano-tokens were at the core of the degradation. In the final Gen 3 sample (also used for the data analysis in Fig. 4 of the main text), the focusing errors were minimized by decreasing the required total refocusing range of the objective and performing an additional calibration step using a Si wafer. The required refocusing range was decreased by doing a touch off for the EBL writing at a fiducial on the part's flat region marked by the nickel nano-beads, as discussed in the Materials and Methods section. The objective focal length had to be decreased by only ~600 μm using this approach (vs. >3 mm previously required when using the markers on the cassette for touch off). Additionally, the "home" position where the lens would refocus between each writing zone was chosen to be at the apex of the toroid. Once the

lens refocused from the nano-beads at the fiducial to the apex of the toroid at the beginning of the writing, the lens only had to refocus at most by ~100 μm, which corresponds to the total sag of the toroid within the active 2 mm by 1.5 mm metaform area. The resulting stitching errors for the Gen 3 part were on the scale of a few tens of nm, which is in a range typical for conventional EBL writing on a flat substrate. As shown in Fig. S3, the corresponding final images do not demonstrate any grid-like diffraction artifacts and provide satisfactory optical performance.

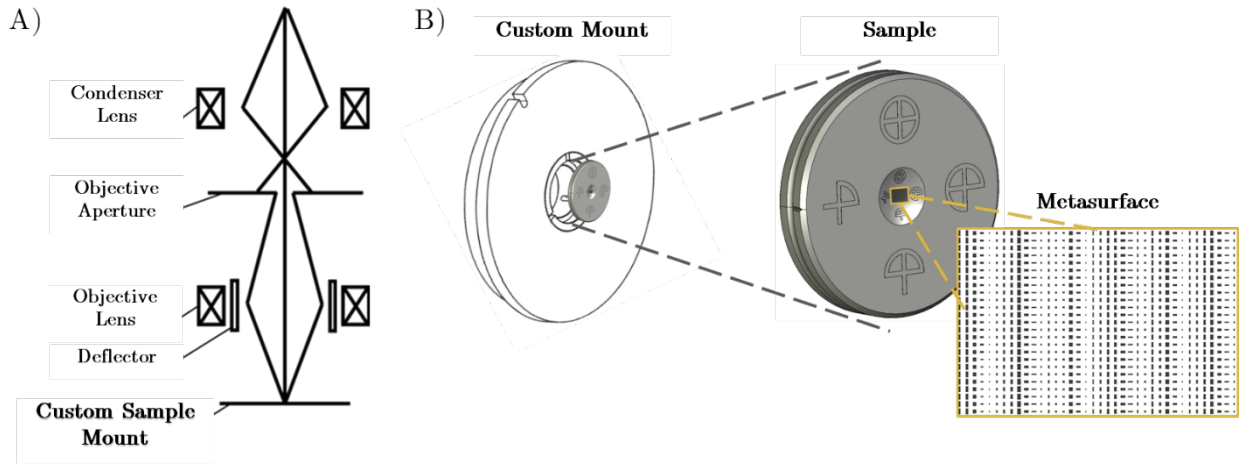

Fig. S1. A diagram of the EBL process used to make the metaform mirror for the imager. **(A)** A simplified sketch of the EBL system (adapted from JEOL USA, Inc.) **(B)** A diagram of the custom cassette used in the EBL machine for writing on a curved substrate. Scaled up insets of the metaform part that fits in the cassette and a set of the metasurface nano tokens are also shown.

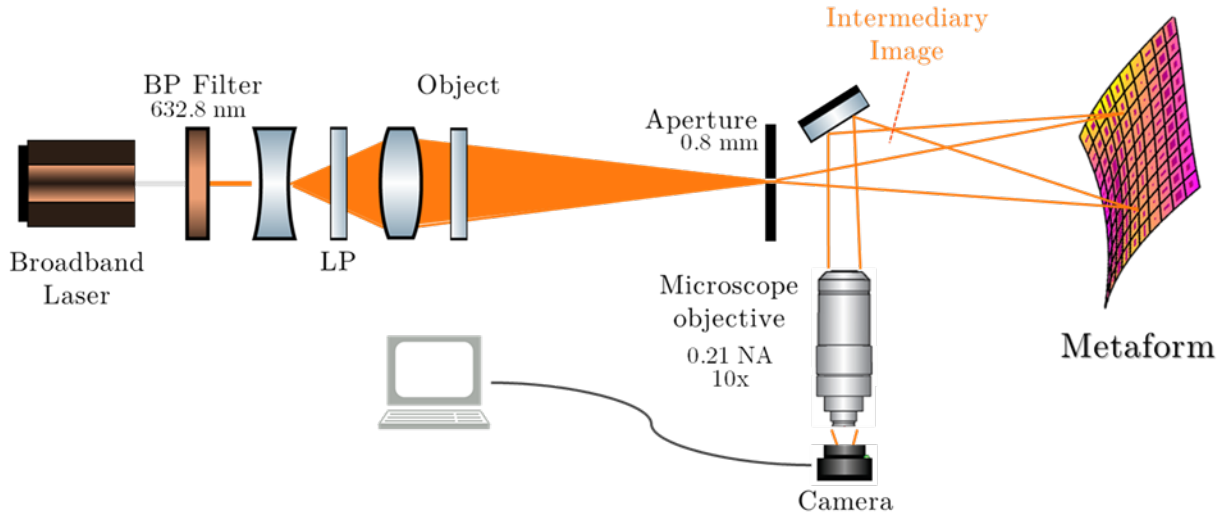

Fig. S2. A diagram of the experimental setup

The setup used to collect the images in Fig. 4 and Fig. S3. The intermediary image is reimaged to a CMOS machine vision camera using a finite conjugate 10X 0.21 NA Mitutoyo microscope objective.

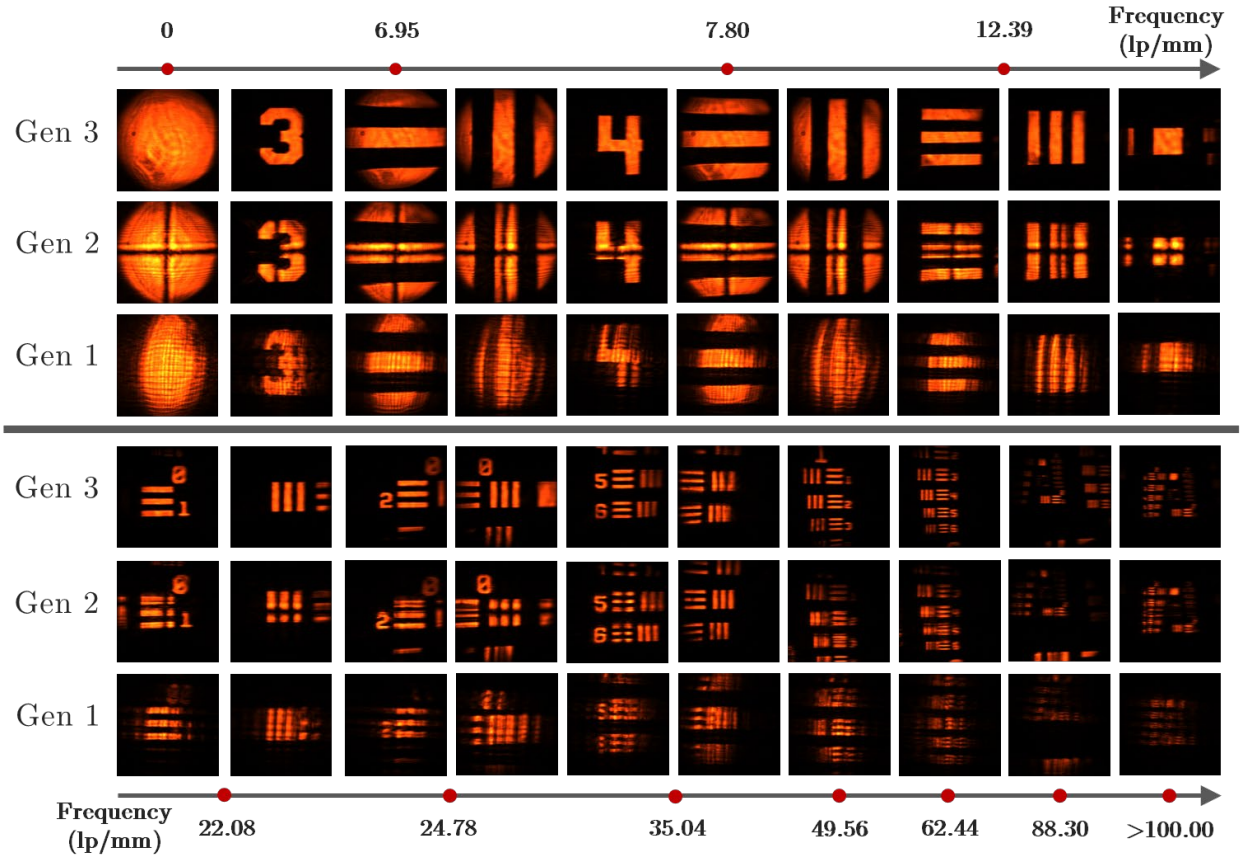

Fig. S3. Experimental imaging results from three different samples Gen 1-3.

Gen 1 is a sample with a metasurface grating clocked 89 degrees from the designed direction and with ~1.5 µm wide stitching/focusing errors between each 62.5 µm by 62.5 µm writing zone. Gen 2 has a decenter error (between the metasurface and the toroid apex) of ±100 µm and ~30 µm stitching errors between each 1 mm by 1 mm stitching zone. Gen 3 is the final part shown in Fig. 3C. A set of different regions of the resolution target imaged via each metaform part is shown. The spatial frequencies of the object range from 0.315 lp/mm to greater than 4.53 lp/mm (or 6.95 lp/mm to greater than 100 lp/mm in image space). The features decrease in size from left to right and from top to bottom.

REFERENCES AND NOTES

1. B. C. Kress, *Optical Architectures for Augmented-, Virtual-, and Mixed-Reality Headsets* (SPIE, 2020).

2. O. Cakmakci, O. A. Martinez, J. Carollo, *Digital Optical Technologies 2019* (International Society for Optics and Photonics, 2019), vol. 11062.

3. H. Huang, H. Hua, High-performance integral-imaging-based light field augmented reality display using freeform optics. *Opt. Express* **26**, 17578–17590 (2018).

4. A. Maimone, A. Georgiou, J. S. Kollin, Holographic near-eye displays for virtual and augmented reality. *ACM Trans. Graph.* **36**, 1–16 (2017).

5. C. Hong, S. Colburn, A. Majumdar, Flat metaform near-eye visor. *Appl. Optics* **56**, 8822–8827 (2017).

6. D. Cheng, Y. Wang, C. Xu, W. Song, G. Jin, Design of an ultra-thin near-eye display with geometrical waveguide and freeform optics. *Opt. Express* **22**, 20705–20719 (2014).

7. A. F. Koenderink, A. Alù, A. Polman, Nanophotonics: Shrinking light-based technology. *Science* **348**, 516–521 (2015).

8. N. A. Rubin, G. D'Aversa, P. Chevalier, Z. Shi, W. T. Chen, F. Capasso, Matrix Fourier optics enables a compact full-Stokes polarization camera. *Science* **365**, eaax1839 (2019).

9. A. Bauer, M. Pesch, J. Muschaweck, F. Leupelt, J. P. Rolland, All-reflective electronic viewfinder enabled by freeform optics. *Opt. Express* **27**, 30597–30605 (2019).

10. A. Arbabi, E. Arbabi, S. M. Kamali, Y. Horie, S. Han, A. Faraon, Miniature optical planar camera based on a wide-angle metasurface doublet corrected for monochromatic aberrations. *Nat. Commun.* **7**, 13682 (2016).

11. M. Khorasaninejad, W. T. Chen, R. C. Devlin, J. Oh, A. Y. Zhu, F. Capasso, Metalenses at visible wavelengths: Diffraction-limited focusing and subwavelength resolution imaging. *Science* **352**, 1190–1194 (2016).

12. E. M. Schiesser, A. Bauer, J. P. Rolland, Effect of freeform surfaces on the volume and performance of unobscured three mirror imagers in comparison with off-axis rotationally symmetric polynomials. *Opt. Express* **27**, 21750–21765 (2019).

13. B. Zhang, G. Jin, J. Zhu, Design method for freeform optical systems containing diffraction gratings. *Opt. Express* **26**, 20792–20801 (2018).

14. J. Reimers, A. Bauer, K. P. Thompson, J. P. Rolland, Freeform spectrometer enabling increased compactness. *Light Sci. Appl.* **6**, e17026 (2017).

15. S.-Q. Li, X. Xu, R. M. Veetil, V. Valuckas, R. Paniagua-Domínguez, A. I. Kuznetsov, Phase-only transmissive spatial light modulator based on tunable dielectric metasurface. *Science* **364**, 1087–1090 (2019).

16. F. Z. Fang, X. D. Zhang, A. Weckenmann, G. X. Zhang, C. Evans, Manufacturing and measurement of freeform optics. *CIRP Ann.* **62**, 823–846 (2013).

17. E. Acosta, J. Sasián, Phase plates for generation of variable amounts of primary spherical aberration. *Opt. Express* **19**, 13171–13178 (2011).

18. N. Yu, F. Capasso, Flat optics with designer metasurfaces. *Nat. Mater.* **13**, 139–150 (2014).

19. A. Bauer, E. M. Schiesser, J. P. Rolland, Starting geometry creation and design method for freeform optics. *Nat. Commun.* **9**, 1756 (2018).

20. M. Born, E. Wolf, *Principles of Optics: 60th Anniversary Edition* (Cambridge Univ. Press, 2019).

21. G. W. Forbes, B. D. Stone, Hamilton's angle characteristic in closed form for generally configured conic and toric interfaces. *J. Opt. Soc. Am. A* **10**, 1270–1278 (1993).

22. O. Cakmakci, B. Moore, H. Foroosh, J. P. Rolland, Optimal local shape description for rotationally non-symmetric optical surface design and analysis. *Opt. Express* **16**, 1583–1589 (2008).

23. G. W. Forbes, Characterizing the shape of freeform optics. *Opt. Express* **20**, 2483–2499 (2012).

24. K. P. Thompson, J. P. Rolland, Freeform optical surfaces: A revolution in imaging optical design. *Optics Photonics News* **23**, 30–35 (2012).

25. J. P. Rolland, M. A. Davies, T. J. Suleski, C. Evans, A. Bauer, J. C. Lambropoulos, K. Falaggis, Freeform optics for imaging. *Optica* **8**, 161–176 (2021).

26. K. Fuerschbach, G. E. Davis, K. P. Thompson, J. P. Rolland, Assembly of a freeform off-axis optical system employing three φ-polynomial Zernike mirrors. *Opt. Lett.* **39**, 2896–2899 (2014).

27. R. Geyl, E. Ruch, R. Bourgois, R. Mercier-Ythier, H. Leplan, F. Riguet, in *International Conference on Space Optics—ICSO 2018* (International Society for Optics and Photonics, 2019), vol. 11180.

28. N. Yu, P. Genevet, M. A. Kats, F. Aieta, J.-P. Tetienne, F. Capasso, Z. Gaburro, Light propagation with phase discontinuities: Generalized laws of reflection and refraction. *Science* **334**, 333–337 (2011).

29. X. Chen, L. Huang, H. Mühlenbernd, G. Li, B. Bai, Q. Tan, G. Jin, C.-W. Qiu, S. Zhang, T. Zentgraf, Dual-polarity plasmonic metalens for visible light. *Nat. Commun.* **3**, 1198 (2012).

30. N. Fang, H. Lee, C. Sun, X. Zhang, Sub-diffraction-limited optical imaging with a silver superlens. *Science* **308**, 534–537 (2005).

31. A. V. Kildishev, A. Boltasseva, V. M. Shalaev, Planar photonics with metasurfaces. *Science* **339**, 1232009 (2013).

32. A. Pors, S. I. Bozhevolnyi, Efficient and broadband quarter-wave plates by gap-plasmon resonators. *Opt. Express* **21**, 2942–2952 (2013).

33. A. Pors, M. G. Nielsen, S. I. Bozhevolnyi, Broadband plasmonic half-wave plates in reflection. *Opt. Lett.* **38**, 513–515 (2013).

34. J. Yang, D. Sell, J. A. Fan, Freeform metagratings based on complex light scattering dynamics for extreme, high efficiency beam steering. *Ann. Phys.* **530**, 1700302 (2018).

35. S. Larouche, Y.-J. Tsai, T. Tyler, N. M. Jokerst, D. R. Smith, Infrared metamaterial phase holograms. *Nat. Mater.* **11**, 450–454 (2012).

36. X. Ni, A. V. Kildishev, V. M. Shalaev, Metasurface holograms for visible light. *Nat. Commun.* **4**, 2807 (2013).

37. A. Zhan, S. Colburn, C. M. Dodson, A. Majumdar, Metasurface freeform nanophotonics. *Sci. Rep.* **7**, 1673 (2017).

38. X. Ni, Z. J. Wong, M. Mrejen, Y. Wang, X. Zhang, An ultrathin invisibility skin cloak for visible light. *Science* **349**, 1310–1314 (2015).

39. S. M. Kamali, A. Arbabi, E. Arbabi, Y. Horie, A. Faraon, Decoupling optical function and geometrical form using conformal flexible dielectric metasurfaces. *Nat. Commun.* **7**, 11618 (2016).

40. C. F. Gauss, *Disquisitiones Generales Circa Superficies Curvas* (Typis Dieterichianis, 1828).

41. B. Kress, T. Starner, A review of head-mounted displays (HMD) technologies and applications for consumer electronics. *Proc. SPIE* **8720**, 87200A (2013).

42. J. P. McGuire Jr, *Emerging Liquid Crystal Technologies V* (International Society for Optics and Photonics, 2010), vol. 7618.

43. D. K. Nikolov, F. Cheng, L. Ding, A. Bauer, A. N. Vamivakas, J. P. Rolland, See-through reflective metasurface diffraction grating. *Opt. Mater. Express* **9**, 4070–4080 (2019).

44. A. L. Kitt, J. P. Rolland, A. N. Vamivakas, Visible metasurfaces and ruled diffraction gratings: A comparison. *Opt. Mater. Express* **5**, 2895–2901 (2015).

45. D. K. Nikolov, F. Cheng, N. Basaran, A. Bauer, J. P. Rolland, A. N. Vamivakas, Long-term efficiency preservation for gradient phase metasurface diffraction gratings in the visible. *Opt. Mater. Express* **8**, 2125–2130 (2018).

46. A. A. Michelson, *Studies in Optics* (Courier Corporation, 1995).

47. J. W. Goodman, *Introduction to Fourier Optics* (Roberts and Company Publishers, 2005).

48. L. G. Cook, Reflective optical triplet having a real entrance pupil, U.S. Patent 4,733,955 (1988).

49. K. Fuerschbach, J. P. Rolland, K. P. Thompson, Theory of aberration fields for general optical systems with freeform surfaces. *Opt. Express* **22**, 26585–26606 (2014).

50. V. Ray, Y. Aida, R. Funakoshi, H. Kato, S. W. Pang, High resolution patterning on nonplanar substrates with large height variation using electron beam lithography. *J. Vacuum Sci. Technol. B* **30**, 06F303 (2012).

51. D. Wilson, P. Maker, R. Muller, P. Mouroulis, J. Backlund, Recent advances in blazed grating fabrication by electron-beam lithography. *Proc. SPIE* **5173**, 51730E (2003).

52. R. Peng, D. Wang, Z. Hu, J. Chen, S. Zhuang, Focal length hysteresis of a double-liquid lens based on electrowetting. *J. Opt.* **15**, 025707 (2013).